Journal of Marine Science and Technology

Volume 24 | Issue 5 Article 5

# BEARING BOUNDARY ELEMENT METHOD BASED ON GEOMETRICALLY SIMILAR ROLLER CONDITIONS

Xia Yang
*Shanxi Provincial Key Laboratory of Metallurgical Device Design Theory and Technology, Taiyuan University of Science and Technology, Taiyuan, P.R. China.*, xiay06@163.com

Ya-Chao Li
*Shanxi Provincial Key Laboratory of Metallurgical Device Design Theory and Technology, Taiyuan University of Science and Technology, Taiyuan, P.R. China.*

Chuang Yan
*Shanxi Provincial Key Laboratory of Metallurgical Device Design Theory and Technology, Taiyuan University of Science and Technology, Taiyuan, P.R. China.*

Guang-ming Liu
*Shanxi Provincial Key Laboratory of Metallurgical Device Design Theory and Technology, Taiyuan University of Science and Technology, Taiyuan, P.R. China.*

Jian-mei Wang
*Shanxi Provincial Key Laboratory of Metallurgical Device Design Theory and Technology, Taiyuan University of Science and Technology, Taiyuan, P.R. China.*

*See next page for additional authors*

# BEARING BOUNDARY ELEMENT METHOD BASED ON GEOMETRICALLY SIMILAR ROLLER CONDITIONS

## Acknowledgements

This study is supported by the National Natural Science Foundation of China (Grant No. 51504157 and 51404159), Natural Science Foundation of Shanxi province (Grant No. 2015021110) and Youth Foundation of Taiyuan University of Science and Technology (Grant No. 20143009).

## Authors

Xia Yang, Ya-Chao Li, Chuang Yan, Guang-ming Liu, Jian-mei Wang, and Hai-lian Gui

Journal of Marine Science and Technology, Vol. 24, No. 5, pp. 938-948 (2016)
DOI: 10.6119/JMST-016-0524-1

# BEARING BOUNDARY ELEMENT METHOD BASED ON GEOMETRICALLY SIMILAR ROLLER CONDITIONS

Xia Yang, Ya-Chao Li, ChuangYan, Guang-ming Liu, Jian-mei Wang, and Hai-lian Gui

Key words: bearing Boundary Element Method, geometrically similar roller conditions, contact pressure, simulation.

## ABSTRACT

To solve the three-dimensional pressure and load distribution of roller bearings, a new boundary element method (BEM) is presented in this report. First, a discrete model of the initial location roller was established, and the other rollers' discrete data could be obtained using geometrically similar conditions of this model. Based on the three-dimensional elastic contact BEM, all of the bearing rollers could be described as one object; therefore, the roller bearing problem of a multi-object contact system could be simplified as the problem of a three-object contact system. Bearing boundary elements were used to realize the discontinuous traction on the contact area, and the Hertz contact theory was used to revise the contact widths between the rollers and the bearing races, including the inner and outer races. A coupling matrix equation was established, and the boundary matrix equation's condensation process was illustrated. A bearing-BEM program was compiled based on geometrically similar roller conditions, in which a four-row tapered roller bearing in a rolling mill was simulated. The bearing contact pressure and load, roller contact widths and number of contact rollers were obtained. Lastly, the simulation result was compared with that of the traditional bearing-BEM (T-BBEM) and the experimental data, which proved the validity and effectiveness of the developed method.

## I. INTRODUCTION

Among the different types of mechanical transmission systems, roller bearings are not only one of the most important parts but also the most easily damaged. An accurate calculation of the distribution of load bearing is extremely important for improving its service life (Waghole and Tiwari, 2014). The friction coefficient of rolling contact is considerably lower than that of the sliding contact, and the roller bearing has an elastohydrodynamic lubrication effect on most operating conditions, i.e., friction is generally not considered when the roller bearing load distribution is studied (Zhou et al., 2006). A roller bearing system is a typical multi-object elastic contact problem. When investigating the roller bearing load distribution, most researchers use both analytical (Wang and Yuan, 2013; Göncz et al., 2013) and numerical methods (Zhang, 2012; Wang and Dai, 2013).

In numerical solutions, because the boundary element method (BEM) with response parameters can be obtained directly on the boundary, the object boundary is only required to divide elements in the elastic state not the global region, and the solving scale is reduced by one dimension. The dimension reduction results in small data preparation and high precision when calculating the elastic contact problems (Segond and Tafreshi, 1998). Using the BEM to solve contact problems, Gun and Gao (2014) proposed a quadratic boundary element formulation for continuously non-homogeneous, isotropic and linear elastic functionally graded material contact problems with friction, in which the punch problem and two cylinders in contact were calculated. Chen (2010) proposed a Taylor Series Multiple BEM for solving 3D multi-body elastic frictional contact problems using a "node-to-surface" contact model, in which a HC roll system was calculated. L. Rodríguez-Tembleque and Abascal (2010) proposed a new and efficient methodology for 3D frictional contact problems based on the Generalized Newton Method using a line search. Gui et al. (2013) proposed a variable elements length theory to determine the change in the contact area in contact problems. Yu (2005) proposed a new mathematical model for the highly nonlinear problem of frictional contact. A programming model, i.e., a multiple BEM, was developed for the 3-D elastic contact with friction to replace the Monte Carlo method. Using the BEM to solve bearing contact problems, Shen et al. (2001) and Shu and Xing (2004) used plate units instead of rollers, which were fixed to the bearing's inner race. The bearing system was simplified into a two-object contact problem within the inner and outer races; instead of looking at the roller displacement, this

*Paper submitted 10/27/15; revised 12/09/15; accepted 05/24/16. Author for correspondence: Xia Yang (e-mail: xiay06@163.com).*
*Shanxi Provincial Key Laboratory of Metallurgical Device Design Theory and Technology, Taiyuan University of Science and Technology, Taiyuan, P.R. China.*

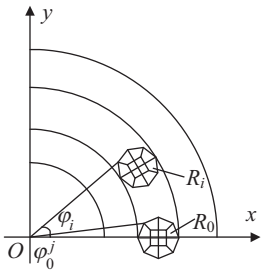


**Fig. 1. Location and geometric relationship of discrete rollers.**

method examines the roller's radial approach value within the inner and outer races, which can then be used to simulate the roller bearing's load distribution.

Because the roller bearing contact problem has multiple small contact areas, there are extremely few literatures analyzing the load distribution of roll bearing using the BEM. Moreover, several simplifications have been performed in the existing literatures, which could not initially realize the full contact models of the bearing inner race, rollers and outer race. The bearing-BEM, which is based on the geometrically similar conditions of rollers known as GSC-BBEM, is proposed in this report. In this method, all of the rollers in the roller bearing are assumed to be elastic contact objects and their elastic deformation can be calculated. Thus, the roller bearing's pressure and load distribution can be simulated more accurately.

## II. GEOMETRICALLY SIMILAR ROLLER CONDITIONS

All rollers in a roller bearing have the same shape and boundary conditions, but their different positions. Therefore, when analyzing a roller bearing with geometrically similar conditions, the discrete model of the original roller (represented by $R_0$) needs to be first established firstly. Fig. 1 depicts a roller in the horizontal position.

The other rollers' node coordinates and element compositions can be calculated based on the node coordinates and element compositions of the original roller's ($R_0$) geometric relation as follows:

$$\begin{cases} x_i^j = r_0^j \cos(\varphi_i + \varphi_0^j) \\ y_i^j = r_0^j \sin(\varphi_i + \varphi_0^j) \\ z_i^j = z_0^j \\ r_0^j = \sqrt{(x_0^i)^2 + (y_0^i)^2} \end{cases} \tag{1}$$

where $x_i^j$, $y_i^j$ and $z_i^j$ represent the coordinate values of the $j$-th node on the $i$-th roller; $r_0^j$ represents the distance from the center of the bearing to the $j$-th node on the original roller; $x_0^j$, $y_0^j$ and $z_0^j$ represent the coordinate values of the $j$-th node on the original roller; $\varphi_i = 2\pi i / n$ represents the angle of the $i$-th roller relative to the original roller; and $\varphi_0^j$ is the angle between the $j$-th node on the original roller and the positive direction of the $x$ axis.

For single-row bearings and multi-row cylindrical bearings, we only need to establish a discrete model of the original roller. For multi-row tapered bearings, the rollers are tapered, and the direction of the two adjacent columns is thus inconsistent. Therefore, the discrete models of the original rollers for both the first and second rows need to be established.

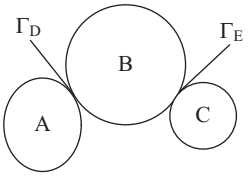


**Fig. 2. Contact schematic of three elastic objects.**

## III. THREE-OBJECT ELASTIC CONTACT BEM WITHOUT FRICTION

Let us consider three line elastomers A, B and C (as illustrated in Fig. 2) that contact each other, and their corresponding boundaries are $\Gamma_A$, $\Gamma_B$ and $\Gamma_C$, respectively. $\Gamma_D$ is the contact boundary of A and B whereas $\Gamma_E$ is the contact boundary of B and C (Yang and Xiao, 2009).

### 1. Contact State

The contact boundaries of $\Gamma_D$ and $\Gamma_E$ are divided into a pre-contact boundary, represented by $\Gamma_{DP}$ and $\Gamma_{EP}$, and a contacted boundary, represented by $\Gamma_{DC}$ and $\Gamma_{EC}$. $\Gamma_F^k$ indicates the non-contact area boundary of the $k$-th object.

When using a condensed method, because the number of unknown quantities is greater than the number of equations, a local coordinate system (represented by $\xi_1, \xi_2, \xi_3$) should be established on the contact area to add equations, and the contact area's unknown quantities can then be solved. The procedure for establishing a local coordinate system can be given as follows: the direction of $\xi_3$ must be the outward normal direction of the contact boundary, and the local coordinate system ($\xi_1, \xi_2, \xi_3$) must meet the right-hand rule. For example, the contact node can be selected from $\Gamma_D$.

On the contacted boundary of $\Gamma_{DC}$, the node contact state can be expressed as follows:

$$\begin{cases} t_{\xi_l}^A = t_{\xi_l}^B = 0, l = 1, 2 \\ t_{\xi_3}^A - t_{\xi_3}^B = 0 \\ u_{\xi_3}^D = u_{\xi_3}^D - (u_{\xi_3}^A + u_{\xi_3}^B) \le 0 \end{cases} \tag{2}$$

On the pre-contact contact boundary of $\Gamma_{DP}$, the node contact state can be expressed as follows:

$$\begin{cases} t_{\xi_l}^{A} = t_{\xi_l}^{B} = 0, l = 1, 2, 3 \\ u_{\xi_3}^{D} > 0 \end{cases} \tag{3}$$

where $t_{\xi_l}^{k}$ is the traction in the $\xi_l$ direction under the local coordinate system of the $k$-th object; $u_{\xi_3}^{k}$ is the displacement in the $\xi_3$ direction under the local coordinate system of the $k$-th object; and $u_{\xi_3}^{D}$ is the initial clearance of the contact node pair on the contact boundary $\Gamma_D$ in $\xi_3$ direction under the local coordinate system.

The contact state equations on the contact boundary $\Gamma_E$ can be similarly presented using Eqs. (2) and (3).

## 2. Boundary Integral Equation

Based on the elastic problem's boundary integral equation and coupling contact state equations, there are three-object boundary integral equations that need to be solved.

For object A,

$$\begin{aligned} & C_{ij}^{A}(X^{A})u_j^{A}(X^{A}) + \int_{\Gamma_F^A} T_{ij}^{*}(X^{A}, Y^{A})u_j^{A}(Y^{A})\mathrm{d}\Gamma \\ & + \int_{\Gamma_D^A} T_{ij}^{*}(X^{A}, Y^{A})u_{\xi_l}^{A}(Y^{A})\alpha_{lj}^{A}(Y^{A})\mathrm{d}\Gamma \\ & - \int_{\Gamma_F^A} U_{ij}^{*}(X^{A}, Y^{A})t_j^{A}(Y^{A})\mathrm{d}\Gamma \\ & - \int_{\Gamma_D^A} U_{ij}^{*}(X^{A}, Y^{A})t_{\xi_3}^{A}(Y^{A})\alpha_{3j}^{A}(Y^{A})\mathrm{d}\Gamma = 0 \end{aligned} \tag{4}$$

For object B,

$$\begin{aligned} & C_{ij}^{B}(X^{B})u_j^{B}(X^{B}) + \int_{\Gamma_F^B} T_{ij}^{*}(X^{B}, Y^{B})u_j^{B}(Y^{B})\,\mathrm{d}\Gamma + \int_{\Gamma_{DP}^B} T_{ij}^{*}(X^{B}, Y^{B})u_{\xi_l}^{B}(Y^{B})\alpha_{lj}^{B}(Y^{B})\mathrm{d}\Gamma \\ & + \int_{\Gamma_{DC}^B} T_{ij}^{*}(X^{B}, Y^{B})u_{\xi_1}^{B}(Y^{B})\alpha_{1j}^{B}(Y^{B})\,\mathrm{d}\Gamma + \int_{\Gamma_{DC}^B} T_{ij}^{*}(X^{B}, Y^{B})u_{\xi_2}^{B}(Y^{B})\alpha_{2j}^{B}(Y^{B})\mathrm{d}\Gamma \\ & + \int_{\Gamma_{DC}^C} T_{ij}^{*}(X^{B}, Y^{B})[u_{\xi_3}^{D} - u_{\xi_3}^{A}(Y^{A})]\alpha_{3j}^{B}(Y^{B})\mathrm{d}\Gamma + \int_{\Gamma_{EP}^B} T_{ij}^{*}(X^{B}, Y^{B})u_{\xi_l}^{B}(Y^{B})\alpha_{lj}^{B}(Y^{B})\mathrm{d}\Gamma \\ & + \int_{\Gamma_{EC}^B} T_{ij}^{*}(X^{B}, Y^{B})u_{\xi_1}^{B}(Y^{B})\alpha_{1j}^{B}(Y^{B})\mathrm{d}\Gamma + \int_{\Gamma_{EC}^B} T_{ij}^{*}(X^{B}, Y^{B})u_{\xi_2}^{B}(Y^{B})\alpha_{2j}^{B}(Y^{B})\mathrm{d}\Gamma \\ & + \int_{\Gamma_{EC}^B} T_{ij}^{*}(X^{B}, Y^{B})[u_{\xi_3}^{E} - u_{\xi_3}^{C}(Y^{B})]\alpha_{3j}^{B}(Y^{B})\mathrm{d}\Gamma - \int_{\Gamma_F^B} U_{ij}^{*}(X^{B}, Y^{B})t_j^{B}(Y^{B})\mathrm{d}\Gamma \\ & - \int_{\Gamma_D^B} U_{ij}^{*}(X^{B}, Y^{B})\,t_{\xi_3}^{A}(Y^{B})\alpha_{3j}^{B}(Y^{B})\mathrm{d}\Gamma - \int_{\Gamma_E^B} U_{ij}^{*}(X^{B}, Y^{B})t_{\xi_3}^{C}(Y^{B})\alpha_{3j}^{B}(Y^{B})\mathrm{d}\Gamma = 0 \end{aligned} \tag{5}$$

For object C,

$$\begin{aligned} & C_{ij}^{C}(X^{C})u_j^{C}(X^{C}) + \int_{\Gamma_F^C} T_{ij}^{*}(X^{C}, Y^{C})u_j^{C}(Y^{C})\mathrm{d}\Gamma \\ & + \int_{\Gamma_E^C} T_{ij}^{*}(X^{C}, Y^{C})u_{\xi_l}^{C}(Y^{C})\alpha_{lj}^{C}(Y^{C})\mathrm{d}\Gamma \\ & - \int_{\Gamma_E^C} U_{ij}^{*}(X^{C}, Y^{C})t_j^{C}(Y^{C})\mathrm{d}\Gamma \\ & - \int_{\Gamma_E^C} U_{ij}^{*}(X^{C}, Y^{C})t_{\xi_3}^{C}(Y^{C})\alpha_{3j}^{C}(Y^{C})\mathrm{d}\Gamma = 0 \end{aligned} \tag{6}$$

where $X^k$ and $Y^k$ represent the source point and the integral point of the $k$-th object, respectively; $t_j^k$ and $u_j^k$ represent the traction and displacement of the $k$-th object in the $j$ direction under the global coordinate system, respectively; $\alpha_{lj}$ is the direction cosine between the $\xi_l$ direction under the local coordinate system and the $x_j$ direction under the global coordinate system; $T_{ij}^{*}$ and $U_{ij}^{*}$ represent the traction and displacement fundamental solutions, respectively; and $u_{\xi_3}^{E}$ represents the initial clearance of the contact nodes on the contact area $\Gamma_E$ in the direction of $\xi_3$ under the local coordinate system.

**Table 1. Revised contact states.**

| ($m$-1)-th / $m$-th | Contacted element | Pre-contact element |
|---|---|---|
| Contacted element | $\sum_{j=1}^{4} t_{\xi_3}^{A,i,j} < 0$ | $\sum_{j=1}^{4} u_{\xi_3}^{A,i,j} + \sum_{j=1}^{4} u_{\xi_3}^{B,i,j} < \sum_{j=1}^{4} u_{\xi_3}^{D,i,j}$ |
| Pre-contact element | $\sum_{j=1}^{4} t_{\xi_3}^{A,i,j} \geq 0$ | $\sum_{j=1}^{4} u_{\xi_3}^{A,i,j} + \sum_{j=1}^{4} u_{\xi_3}^{B,i,j} \geq \sum_{j=1}^{4} u_{\xi_3}^{D,i,j}$ |

## 3. Contact Criteria

Because it is highly non-linear, when calculating the contact problem, the contact area initially needs to be assumed, and an iterative algorithm is then used for an accurate calculation. For the $i$-th contact element of object A, Table 1 is used

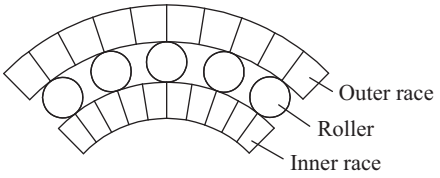


**Fig. 3. Schematic of the discrete inner and outer races.**

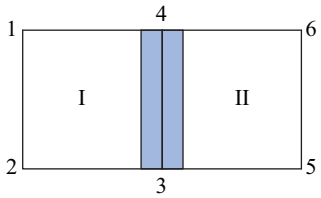


**Fig. 4. Constituent nodes and elements of a contact group.**

to revise the contact states at the ($m$-1)-th and $m$-th processes of iteration.

For object A, the number of contacted elements at the $m$-th and ($m$-1)-th iterations are $N_{ADC}^{m}$ and $N_{ADC}^{m-1}$, respectively. Similarly, for object C, the number of contacted elements within two iterations are $N_{CEC}^{m}$ and $N_{CEC}^{m-1}$. The convergence condition of iteration can be given as follows:

$$\begin{cases} N_{ADC}^{m} = N_{ADC}^{m-1} \\ N_{CEC}^{m} = N_{CEC}^{m-1} \end{cases}$$

## IV. BEARING-BEM

### 1. Discrete Model for the Inner and Outer Bearing Races

Each roller has two contact areas, i.e., contact areas with both the inner and outer races of the bearing. The bearing's inner and outer races contact with $n$ rollers; therefore, the contact areas of both races can be considered as one single contact area, which are divided into $n$ groups. In the discrete model depicted in Fig. 3, the contact nodes and the contact elements start from $\varphi = 0$ (the position of roller $R_0$, as indicated in Fig. 1) counterclockwise.

A contact group is illustrated in Fig. 4.

As seen in Fig. 4, one contact group contains two elements and six nodes. Both elements are contact elements; of the six nodes, the third and fourth are contact nodes while the others are non-contact nodes. The shaded part of the figure indicates the contact width between the rollers and the inner or outer race.

### 2. Bearing Boundary Element

As indicated in Figs. 3 and 4, traction exists only in positions that contact the rollers in contact areas of the inner and outer races. Therefore, bearing boundary elements are used to solve

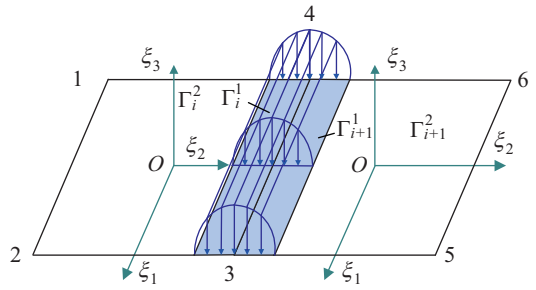


**Fig. 5. Schematic plan of bearing boundary sub-elements.**

the discontinuous problem of traction in both the inner and outer races along the circumferential directions (Yang et al., 2014).

One contact group contains two bearing boundary elements, as indicated in Fig. 5. Bearing boundary element I represents the bearing boundary element on the left side, and bearing boundary element II represents the bearing boundary element on the right side. One bearing boundary element is divided into two sub-elements, there is continuous traction on the sub-elements of $\Gamma_i^1$ and $\Gamma_{i+1}^1$, and there is zero traction on the sub-elements of $\Gamma_i^2$ and $\Gamma_{i+1}^2$. Assuming a normal traction on the sub-elements of $\Gamma_i^1$ and $\Gamma_{i+1}^1$ presents a parabolic distribution along the width direction and a linear distribution along the length direction.

The distribution of traction on the sub-elements of $\Gamma_i^1$ and $\Gamma_{i+1}^1$ can be given as follows:

$$t_{\mathrm{I}}^{i} = t_{\Pi}^{i+1} = \sum_{j=3}^{4} (1+(-1)^j \xi_1)(\xi_2 - \xi_2^0)^2 t_i^j / 2(1-\xi_2^0) \qquad (7)$$

where $\xi_2^0$ is the length in the $\xi_2$ direction of the inner side of the sub-elements $\Gamma_i^1$ and $\Gamma_{i+1}^1$ on the bearing boundary element; and $t_{\mathrm{I}}^{i}$ and $t_{\Pi}^{i+1}$ represent the traction on the sub-elements $\Gamma_i^1$ and $\Gamma_{i+1}^1$ for the bearing boundary elements I and II, respectively.

The aspect ratio of the sub-elements $\Gamma_i^1$ and $\Gamma_{i+1}^1$ is so large that larger errors will result during the integral calculation. Therefore, it needs to be further divided into multiple bearing boundary micro-elements (Shu and Xing, 2004), and the bearing boundary micro-element aspect ratio should be limited to less than 3. The aspect ratio of the bearing boundary micro-element with a singular point is equal to one. The schematic plan of the bearing boundary micro-elements is illustrated in Fig. 6.

Each bearing boundary micro-element's area is $\xi_a \le \xi_1 \le \xi_b$ and $\eta_a \le \xi_2 \le \eta_b$. A Gaussian integration should be performed under area conditions of $-1 \le \xi \le 1$ and $-1 \le \eta \le 1$. Therefore, the coordinates of all of the bearing boundary micro-elements can to be transformed as follows

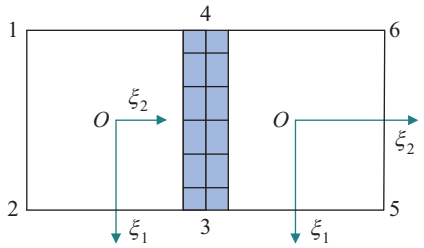


**Fig. 6. Schematic plan of the bearing boundary micro-elements.**

$$\begin{cases} \xi_1 = \dfrac{\xi_a - \xi_b}{2}\xi + \dfrac{\xi_a + \xi_b}{2} \\ \xi_2 = \dfrac{\eta_b - \eta_a}{2}\eta + \dfrac{\eta_b + \eta_a}{2} \end{cases} \tag{8}$$

## 3. Coupling Matrix Equation

When integrating the coupling boundary integral Eqs. from (4) to (6), the known boundary quantities and corresponding impact coefficients can be placed on the right-hand side of the equation, and the unknown boundary quantities and corresponding impact coefficients can be placed on the left. The discrete boundary integral equation can be written as follows:

$$[\boldsymbol{Y}]^k \{\boldsymbol{x}\}^k = \{\boldsymbol{b}\}^k,\ k = \text{A, B, C} \tag{9}$$

where $\boldsymbol{Y}$ is the influence coefficient matrix of the unknown quantities; $\boldsymbol{x}$ is the vector of the unknown quantities; and $\boldsymbol{b}$ is the product vector between the known quantities and the corresponding coefficients.

Because the rolling friction coefficient is small, friction cannot be considered when studying the roller bearing load distribution. All bearing rollers can be described as one object; therefore, the system of roller bearing can be simplified to a three-object contact problem without friction. A is the inner race contact object, B is the contact object of all rollers and C is the outer race contact object.

The boundary integral equation of the $k$-th roller can be given as follows:

$$C_{ij}^{\mathrm{R}_k}(X^{\mathrm{R}_k})u_j^{\mathrm{R}_k}(X^{\mathrm{R}_k}) + \int_{\Gamma^{\mathrm{R}_k}} T_{ij}^*(X^{\mathrm{R}_k}, Y^{\mathrm{R}_k})u_j^{\mathrm{R}_k}(Y^{\mathrm{R}_k})\mathrm{d}\Gamma - \int_{\Gamma^{\mathrm{R}_k}} U_{ij}^*(X^{\mathrm{R}_k}, Y^{\mathrm{R}_k})t_j^{\mathrm{R}_k}(Y^{\mathrm{R}_k})\mathrm{d}\Gamma = 0$$

The bearing system's matrix equation can be obtained when the boundary integral equation of the rollers has been coupled with the inner and outer race as follows:

$$\begin{bmatrix} \boldsymbol{H}^{\mathrm{AF}} & -\boldsymbol{G}^{\mathrm{AF}} & 0 & 0 & 0 & 0 & \\ 0 & 0 & \boldsymbol{H}^{\mathrm{BF}} & -\boldsymbol{G}^{\mathrm{BF}} & 0 & 0 & \boldsymbol{A} \\ 0 & 0 & 0 & 0 & \boldsymbol{H}^{\mathrm{CF}} & -\boldsymbol{G}^{\mathrm{CF}} & \end{bmatrix} \begin{bmatrix} \boldsymbol{u}^{\mathrm{AF}} \\ \boldsymbol{t}^{\mathrm{AF}} \\ \boldsymbol{u}^{\mathrm{BF}} \\ \boldsymbol{t}^{\mathrm{BF}} \\ \boldsymbol{u}^{\mathrm{CF}} \\ \boldsymbol{t}^{\mathrm{CF}} \\ \boldsymbol{x} \end{bmatrix} = \begin{bmatrix} -\boldsymbol{H}^{\mathrm{AF}} & \boldsymbol{G}^{\mathrm{AF}} & 0 & 0 & 0 & 0 & 0 & 0 \\ 0 & 0 & -\boldsymbol{H}^{\mathrm{BF}} & \boldsymbol{G}^{\mathrm{BF}} & -\boldsymbol{H}_{\xi_3}^{\mathrm{BDC}} & -\boldsymbol{H}_{\xi_3}^{\mathrm{BEC}} & 0 & 0 \\ 0 & 0 & 0 & 0 & 0 & 0 & -\boldsymbol{H}^{\mathrm{CF}} & \boldsymbol{G}^{\mathrm{CF}} \end{bmatrix} \begin{bmatrix} \overline{\boldsymbol{u}}^{\mathrm{AF}} \\ \overline{\boldsymbol{t}}^{\mathrm{AF}} \\ \overline{\boldsymbol{u}}^{\mathrm{BF}} \\ \overline{\boldsymbol{t}}^{\mathrm{BF}} \\ \boldsymbol{u}_{\xi_3}^{\mathrm{D}} \\ \boldsymbol{u}_{\xi_3}^{\mathrm{E}} \\ \overline{\boldsymbol{u}}^{\mathrm{CF}} \\ \overline{\boldsymbol{t}}^{\mathrm{CF}} \end{bmatrix} \tag{10}$$

$$\boldsymbol{A} = \begin{bmatrix} \boldsymbol{H}^{\mathrm{ADP}} & 0 & 0 & 0 & \boldsymbol{H}_{\xi_1}^{\mathrm{ADC}} & \boldsymbol{H}_{\xi_2}^{\mathrm{ADC}} & 0 & 0 & 0 & 0 & 0 & \boldsymbol{H}_{\xi_3}^{\mathrm{ADC}} & 0 & -\boldsymbol{G}_{\xi_3}^{\mathrm{ADC}} & 0 \\ 0 & \boldsymbol{H}^{\mathrm{BDP}} & \boldsymbol{H}^{\mathrm{BEP}} & 0 & 0 & 0 & \boldsymbol{H}_{\xi_1}^{\mathrm{BDC}} & \boldsymbol{H}_{\xi_2}^{\mathrm{BDC}} & \boldsymbol{H}_{\xi_1}^{\mathrm{BEC}} & \boldsymbol{H}_{\xi_2}^{\mathrm{BEC}} & 0 & 0 & \boldsymbol{H}_{\xi_3}^{\mathrm{BDC}} & \boldsymbol{H}_{\xi_3}^{\mathrm{BEC}} & -\boldsymbol{G}_{\xi_3}^{\mathrm{BDC}} & -\boldsymbol{G}_{\xi_3}^{\mathrm{BEC}} \\ 0 & 0 & 0 & \boldsymbol{H}^{\mathrm{DEP}} & 0 & 0 & 0 & 0 & 0 & 0 & \boldsymbol{H}_{\xi_1}^{\mathrm{CEC}} & \boldsymbol{H}_{\xi_2}^{\mathrm{CEC}} & 0 & \boldsymbol{H}_{\xi_3}^{\mathrm{CEC}} & 0 & -\boldsymbol{G}_{\xi_3}^{\mathrm{CEC}} \end{bmatrix} \tag{11}$$

$$\boldsymbol{x} = \left[ \boldsymbol{u}^{\mathrm{ADP}}\ \boldsymbol{u}^{\mathrm{BDP}}\ \boldsymbol{u}^{\mathrm{BEP}}\ \boldsymbol{u}^{\mathrm{CEP}}\ \boldsymbol{u}_{\xi_1}^{\mathrm{ADC}}\ \boldsymbol{u}_{\xi_2}^{\mathrm{ADC}}\ \boldsymbol{u}_{\xi_1}^{\mathrm{BDC}}\ \boldsymbol{u}_{\xi_2}^{\mathrm{BDC}}\ \boldsymbol{u}_{\xi_1}^{\mathrm{BEC}}\ \boldsymbol{u}_{\xi_2}^{\mathrm{BEC}}\ \boldsymbol{u}_{\xi_1}^{\mathrm{CEC}}\ \boldsymbol{u}_{\xi_2}^{\mathrm{CEC}}\ \boldsymbol{u}_{\xi_3}^{\mathrm{ADC}}\ \boldsymbol{u}_{\xi_3}^{\mathrm{CEC}}\ \boldsymbol{t}_{\xi_3}^{\mathrm{ADC}}\ \boldsymbol{t}_{\xi_3}^{\mathrm{CEC}} \right]^{\mathrm{T}} \tag{12}$$

where, as indicated in Eq. (11), $\boldsymbol{A}$ is the coefficient matrix of the unknown quantities in the contact area. As depicted in Eq. (12), the vector of $\boldsymbol{x}$ is the unknown quantities in the contact area.

Object B represents all rollers

$$\boldsymbol{H}^{\mathrm{BDP}} = \begin{bmatrix} \boldsymbol{H}_1^{\mathrm{RDP}} & 0 & 0 \ldots & 0 \\ 0 & \boldsymbol{H}_2^{\mathrm{RDP}} & 0 \ldots & 0 \\ \ldots & & & \\ 0 & 0 & 0 \ldots & \boldsymbol{H}_n^{\mathrm{RDP}} \end{bmatrix} \tag{13}$$

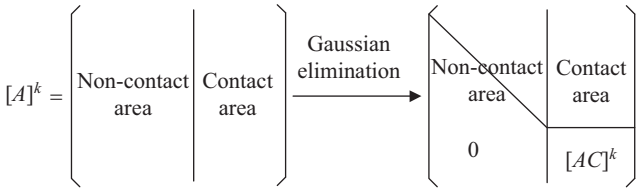


**Fig. 7. Gaussian elimination process.**

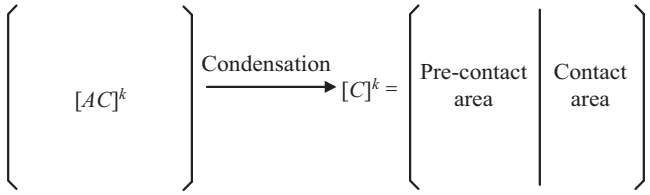


**Fig. 8. Condensation process.**

$$\boldsymbol{u}^{\mathrm{BDP}} = \left[ \boldsymbol{u}_1^{\mathrm{RDP}} \ \boldsymbol{u}_2^{\mathrm{RDP}} \ \ldots \ \boldsymbol{u}_n^{\mathrm{RDP}} \right] \tag{14}$$

The forms of $\boldsymbol{H}^{\mathrm{BEP}}$, $\boldsymbol{H}_{\xi_1}^{\mathrm{BDC}}$, $\boldsymbol{H}_{\xi_2}^{\mathrm{BDC}}$, $\boldsymbol{H}_{\xi_1}^{\mathrm{BEC}}$, $\boldsymbol{H}_{\xi_2}^{\mathrm{BEC}}$, $\boldsymbol{H}_{\xi_3}^{\mathrm{BDC}}$, $\boldsymbol{H}_{\xi_3}^{\mathrm{BEC}}$, $\boldsymbol{G}_{\xi_3}^{\mathrm{BDC}}$ and $\boldsymbol{G}_{\xi_3}^{\mathrm{BEC}}$ in Eq. (11) are the same as those in Eq. (13), and the forms of $\boldsymbol{u}^{\mathrm{BEP}}$, $\boldsymbol{u}_{\xi_1}^{\mathrm{BDC}}$, $\boldsymbol{u}_{\xi_2}^{\mathrm{BDC}}$, $\boldsymbol{u}_{\xi_1}^{\mathrm{BEC}}$ and $\boldsymbol{u}_{\xi_2}^{\mathrm{BEC}}$ in Eq. (12) are the same as those in Eq. (14).

In Eqs. (10) to (14), $\boldsymbol{H}$ and $\boldsymbol{G}$ represent the coefficient matrix of the displacement and traction, respectively, superscripts $k$DC and $k$EC represent the coefficient matrix and the unknown quantities of the $k$-th object on the contacted area, respectively, $k$DP and $k$EP represent the coefficient matrix and the unknown quantities of the $k$-th object on the pre-contact area, respectively, $k$F represents the coefficient matrix and parameters of the $k$-th object on the non-contact area, $\boldsymbol{H}_i^{\mathrm{RDP}}$ represents the displacement influence coefficient matrix of the $i$-th roller on the pre-contact area and $\boldsymbol{u}_i^{\mathrm{RDP}}$ represents the displacement of the $i$-th roller on the pre-contact area.

## 4. Condensation Solving Process

Using the numerical method to solve the boundary integral equation, the boundary must be dispersed into elements with the element node indicating the displacement and traction on the boundary (Yang and Xiao, 2009).

*1) Gaussian Elimination*

For the three-object coefficient matrix, represented by $[\boldsymbol{A}]^k$, the Gaussian elimination can be used until the contact area is reached. Then, the elements from the three objects that have been eliminated can be removed, and a new matrix equation can be re-formed, as represented by $[\boldsymbol{AC}]^k$. Fig. 7 illustrates the Gaussian elimination process.

*2) Condensation*

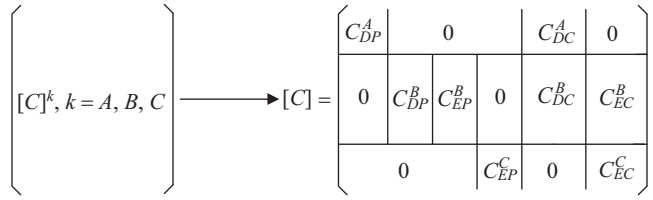


**Fig. 9. Coupling process.**

The impact coefficients of the contacted area can be placed behind the pre-contact area (Yang et al., 2014). The condensed coefficient matrix of the contact area represented by $[\boldsymbol{C}]^k$ can be obtained when a condensation treatment for the contact area's coefficient matrix $[\boldsymbol{AC}]^k$ has been performed. Fig. 8 illustrates the condensation process.

*3) Coupling*

Based on the contact state equations, the coupling coefficient matrix of the contact area represented by $[\boldsymbol{C}]$ can be obtained by coupling the condensation coefficient matrix $[\boldsymbol{C}]^k$. This matrix includes the displacement of the contact area and the impact coefficient of traction. Furthermore, the impact coefficients of the contacted area can be placed behind the pre-contact area. Fig. 9 depicts the coupling process.

Using the coupling coefficient matrix $[\boldsymbol{C}]$ and the corresponding matrix equation, a one-step increment iteration's displacement and traction of the contact area under the local coordinate system can be obtained. Then, the contact state can be determined based on those results, and the next step of incremental solving can be performed until convergence occurs. Lastly, the unknown quantities of the non-contact area can be solved with the general matrix equation and the calculated result of the contact area.

## 5. Revise the Contact Widths between Rollers and Bearing Races

For a highly non-linear bearing system, the contact widths between the rollers and the bearing races, including the inner and outer races, need to be assumed during the calculation process. The Hertz contact theory can be used as a revision basis when the iterative algorithm is used to revise the contact width between each roller in contact and the inner or outer race. The actual contact width is eventually obtained, and the load bearing distribution can be obtained using the actual width (Xiao et al., 2010).

First, a half-width of the contact represented by $b_0$ can be assumed. The contact pressure value of all nodes can be obtained after the first iteration. Then, the total load on the bearing's sub-elements can be calculated. For one contact group (as indicated in Fig. 4), after the calculation, it is possible to obtain the pressure values of every contact node that is on the $i$-th element; which can be represented by $t_k^{i,j}$ (the load of the $j$-th node on the $i$-th element in the direction of $k$). The discrete form of the resultant load on the bearing boundary

sub-elements can be given as follows:

$$T_k^{i,\mathrm{I}} = T_k^{i+1,\Pi} = \sum_{m=1}^{n}\sum_{r=1}^{l}\sum_{j=3}^{4}\left[\phi^j(\xi_1,\xi_2)\omega_1^r\omega_2^r\left|J\left(\xi_1,\xi_2\right)\right|t_k^{i,j}\right] \quad (15)$$

The total load on the outward normal direction of the element, which is also known as 'the positive contact pressure', can be given as follows:

$$T_{\xi_3}^{i,\mathrm{I}} = T_{\xi_3}^{i,j+1} = \sum_{k=1}^{3} T_k^{i,1}\alpha_{3k} \quad (16)$$

where $n$ represents the number of bearing boundary micro-elements on the sub-element of $\Gamma_i^1$; $l$ represents the number of Gaussian integration points; $\omega_1$ and $\omega_2$ represent the weight coefficients of the corresponding integral points; $\xi_1$ and $\xi_2$ represent the coordinates of the Gaussian integral points, $\phi$ represents the shape function; $J$ represents the Jacobi value; and $\alpha_{3k}$ represents the direction cosine in the direction of $\xi_3$ under the global coordinate system.

For cylindrical or tapered roller bearings, the Hertz contact theory can be used. The contact widths between the rollers and the bearing races can be expressed as follows (Bai and Liu, 1996):

$$\begin{cases} b_{\mathrm{i}} = 1.522\sqrt{\dfrac{T_{\xi_3}^{i,\mathrm{I}} l R R_{\mathrm{i}}}{E_{\mathrm{i}}(R+R_{\mathrm{i}})l'}} \\ b_{\mathrm{o}} = 1.522\sqrt{\dfrac{T_{\xi_3}^{i,\mathrm{I}} R R_{\mathrm{o}}}{E_{\mathrm{o}}(R_{\mathrm{o}}-R)l'}} \end{cases} \quad k = \mathrm{I},\ \mathrm{II} \quad (17)$$

where $b_{\mathrm{i}}$ and $b_{\mathrm{o}}$ represent the contact half-widths between the rollers and inner or outer races, respectively; $R_{\mathrm{i}}$ represents the outer radius of the inner race; $R_{\mathrm{o}}$ represents the inner radius of the outer race; $R$ represents the radius of the rollers (for tapered roller bearings, take the average radius); and $l'$ represents the effective length of the rollers.

The contact half-width of each roller can be obtained using Eq. (17). Using the new contact half-widths, the integral calculation and iterative solution are performed until the given convergence criterion is satisfied. Thus, the contact widths for all of the rollers obtained at this time are true.

The convergence criterion can be given as follows:

$$\left|b_1 - b_0\right| \le \varepsilon$$

where $b_1$ represents the contact half-widths between the rollers in contact and the inner or outer race after the Hertz contact theory has been revised; and $\varepsilon$ represents an infinitesimally small positive value.

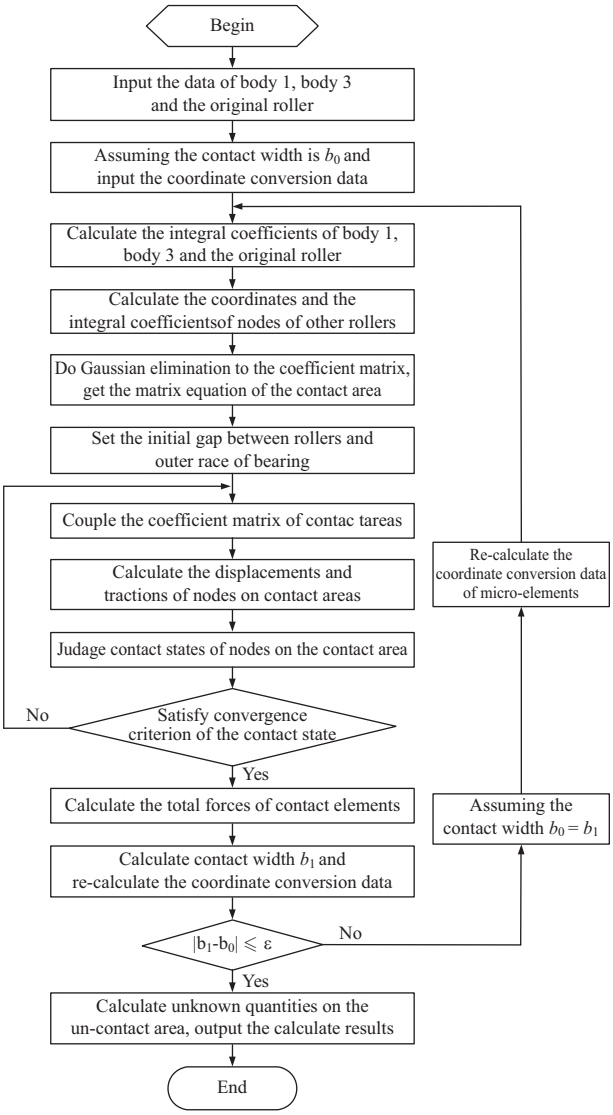


**Fig. 10. Computation flow chart.**

## 6. Computation Flow Chart

With geometrically similar conditions, the discrete model of the original location roller is used to calculate the discrete models of rollers at other locations, the Hertz contact theory is used to revise the contact width between the rollers and bearing races, and the bearing boundary elements are used to simulate the contact elements of the bearing system. The computation flow chart for the bearing-BEM based on geometrically similar roller conditions is depicted in Fig. 10. The numerical BEM algorithm for bearing can be briefly summarized as follows:

(1) Input the coordinates of the nodes, composition of elements and boundary conditions of body 1, body 3 and the original roller.
(2) Assuming the contact width is $b_0$, input the coordinate conversion data of the bearing boundary micro-elements.

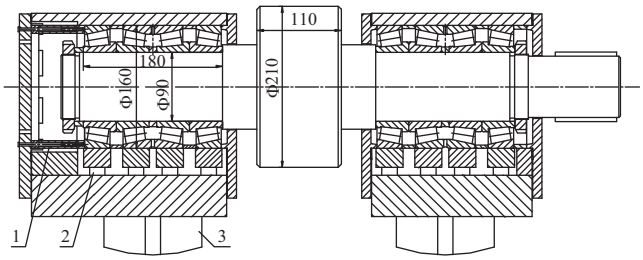


1-Axial force sensor; 2-Radial force sensor; 3-Cylinder cushion

**Fig. 11. Bearing assembly drawing on the work side of the bottom roll.**

(3) Calculate the integral coefficients of body 1, body 3 and the original roller.
(4) Calculate the coordinates and the integral coefficients of the nodes of the other rollers
(5) Perform a Gaussian elimination on the coefficient matrixes to obtain the matrix equations of the contact areas.
(6) Set the initial gap between the rollers and the outer race of the bearing.
(7) Couple the coefficient matrixes of the contact areas and calculate the displacements and tractions of the nodes on the contact areas.
(8) Determine whether the criterions of the contact states of the nodes on the contact areas are satisfied. If yes, then go to step (9). Otherwise, go to step (7).
(9) Calculate the total forces of the contact elements with traction and the contact width $b_0$ of the contact nodes. Calculate the contact width $b_1$ using the Hertz contact theory and re-calculate the coordinate conversion data of the bearing boundary micro-elements.
(10) Determine whether the convergence criterion is satisfied. If $|b_1 - b_0| \le \varepsilon$ , then go to step (11). Otherwise, let $b_0 = b_1$ and go to step (3).
(11) Calculate the unknown quantities on the un-contact areas, and output the calculated results.

## V. NUMERICAL EXAMPLE

### 1. Experimental Data

The load distribution experiment of the four-row tapered bearing with the shaft block direct measure method was performed on a two-roll experimental rolling mill (Yang et al., 2014). The primary technical parameters of the mill can be provided as follows: roll diameter is 210 mm, top roll body length is 150 mm, bottom roll body length is 110 mm, and di ameter of the roll neck is 90 mm. Fig. 11 depicts the bearing assembly drawing on the work side of the bottom roll. Fig. 12 and Fig. 13 depict the pictures of the experimental rolling mill and the experimental data acquisition system respectively.

An aluminum plate rolling experiment was conducted using the experimental conditions as follows: rolling speed of 0.2 m/s, width of the aluminum plate of 40 mm and length of the aluminum plate of 200 mm.

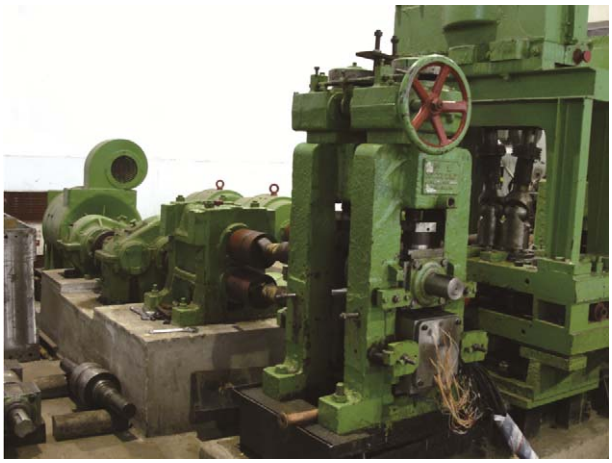

**Fig. 12. Experimental rolling mill.**

**Fig. 13. Experimental data acquisition system.**

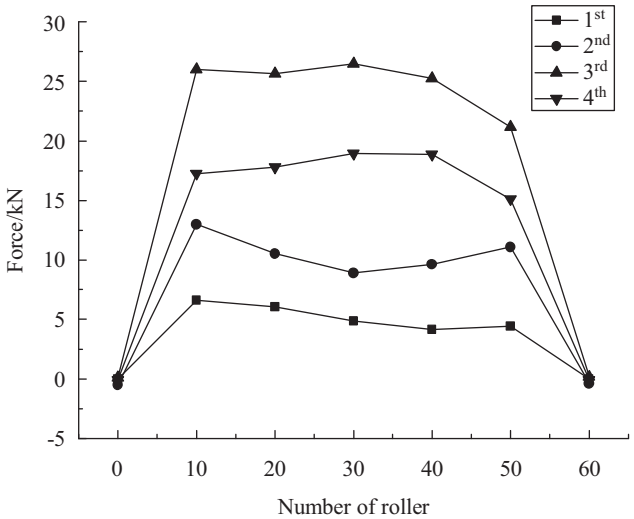


**Fig. 14. Distribution of the radial force for the work side bearing.**

The four rows bearing the radial load distribution on the operating side are illustrated in Fig. 14. It can be seen from the

**Table 2. Discrete data.**

| Component | Total | | Contact area | |
|---|---|---|---|---|
| | *Node* | *Element* | *Node* | *Element* |
| Shaft block | 1000 | 1000 | 160 | 160 |
| Mill roll | 1034 | 1032 | 160 | 160 |
| Rollers | 74 × 80 | 72 × 80 | 4 × 80 | 4 × 80 |
| Total of GSC-BBEM | 7954 | 7792 | 640 | 640 |
| Total of T-BBEM | 2034 | 2032 | 320 | 320 |

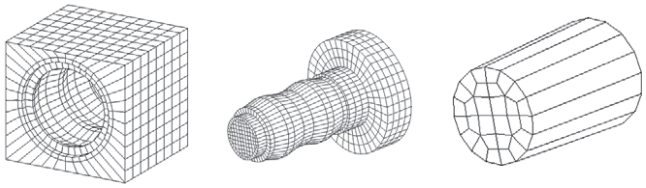

(a) Shaft block (b) Mill roll (c) Original roller

**Fig. 15. Discrete models.**

figure that the second row bears the maximum load, followed by the first row. The calculated rolling force is 147.6 kN.

## 2. Numerical Example

One half of the bottom roll system is used as the calculation model, as indicated in Fig. 11. The modulus of elasticity for the mill roll, shaft block and rollers is 210000 MPa, the Poisson ratio is 0.3, and the bearing size is Φ90 mm / Φ160 mm × 180 mm. The simulation was performed using the geometrically similar conditions bearing-BEM (GSC-BBEM) and the traditional bearing-BEM (T-BBEM).

*1) Simulation Results with GSC-BBEM*

The structure and geometry of the calculation model can be simplified as follows:

There are 20 rollers on one circle of bearing. One circle of the inner race and outer race have been divided into 40 bearing boundary elements with the rollers at the bottom of the first and second columns as the original positions. The rollers at the bottom of each column are numbered as zero. Going anti-clockwise, the roller numbers are negative; going clockwise, the numbers are positive.

The bearing contact angle is 15°, the tapered roller half-cone angle is 2°. The axial arrangement of nodes starts moving from the operating side to the mill roll side.

The mill roll is simplified to be a cantilever beam, and the fixed end is a contact position between the mill roll and a rolled piece. The rolled piece's width is 40 mm; the rolling force is 147.6 kN; reaction force is exerted at the corresponding position of the pressure screw on top of the shaft block. An axially fixed constraint is exerted at the corresponding position of the corresponding axial tailgate on the shaft block.

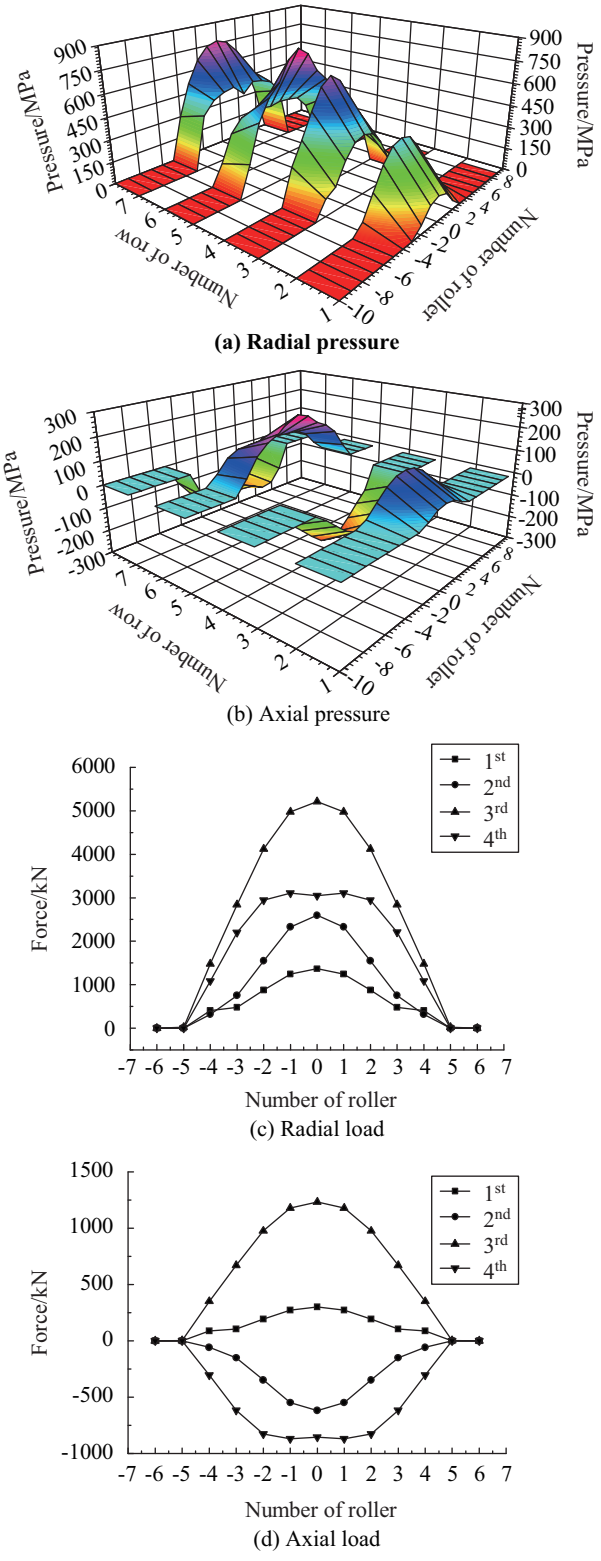


**Fig. 16. Pressure and load distribution of the outer race.**

An axially force is applied to the end surface of the mill roll's operating-side.

The discrete models are illustrated in Fig. 15. The discrete data are listed in Table 2.

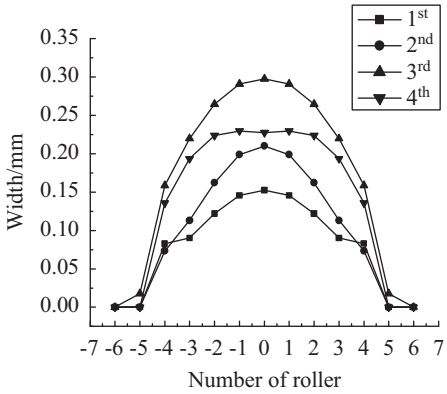


**Fig. 17. Contact width of the rollers.**

The load and pressure distribution of the load-bearing inner and outer races are essentially the same, i.e., the load and pressure of the load-bearing inner races are only slightly larger than those of the outer races. Therefore, only the distribution of the load-bearing outer race is depicted in Fig. 16.

The radial pressure, axial pressure, radial load and axial load of the load-bearing outer race are illustrated in Fig. 16. From Fig. 16, it can be seen that the initial position of the roller on the third column bearing, which is near the mill roll, bears the maximum radial pressure and load of 837.96 MPa and 5215.37 N, respectively. The directions of the axial pressure and axial load borne by rollers at the first and third columns point to the operating side whereas that of the second and fourth columns point to the mill roll. The direction of the axial pressure and axial load of the four-columns tapered bearings is the same as the taper distribution. The negative values in the axial pressure and axial load distribution figures indicate that their direction points to the mill roll side.

The contact widths of the rollers are depicted in Fig. 17. The contact width of each roller is the same as the radial load distribution, and the contact widths between the rollers and the outer race are slightly larger than the widths between the rollers and the inner race. This result conforms to the Hertz's contact theory. Furthermore, the maximum width of the contact roller is 0.298 mm.

*2) Simulation Results with T-BBEM*

The structure and geometry of the calculation models have been simplified as the GSC-BBEM; however, one difference is that the rollers have been simplified into a plate unit with infinite stiffness. The Hertz formula is used to calculate the contact deformation of the plate units. The plate units are considered to be fixed on the inner race (Xiao, 2010).

The discrete models are depicted in Figs. 15(a) and (b). The discrete data of the shaft block and mill roll is listed in Table 2.

Figs. 18(a) and (b) depict the radial and axial load distribution of the rollers for the numerical calculation using the T-BBEM, respectively.

Table 3 provides a comparison of the simulation results and the test results on the work side.

**Table 3. Comparison of experimental results with simulated results.**

| Row number | 1st row | 2nd row | 3rd row | 4th row |
|---|---|---|---|---|
| Experimental results | 10.05% | 16.49% | 40.79% | 32.67% |
| GSC-BBEM | 9.63% | 16.95% | 43.57% | 29.85% |
| Errors | 4.18% | 2.79% | 6.82% | 9.73% |
| T-BBEM | 9.89% | 14.05% | 43.47% | 32.59% |
| Errors | 1.59% | 14.80% | 6.57% | 0.24% |

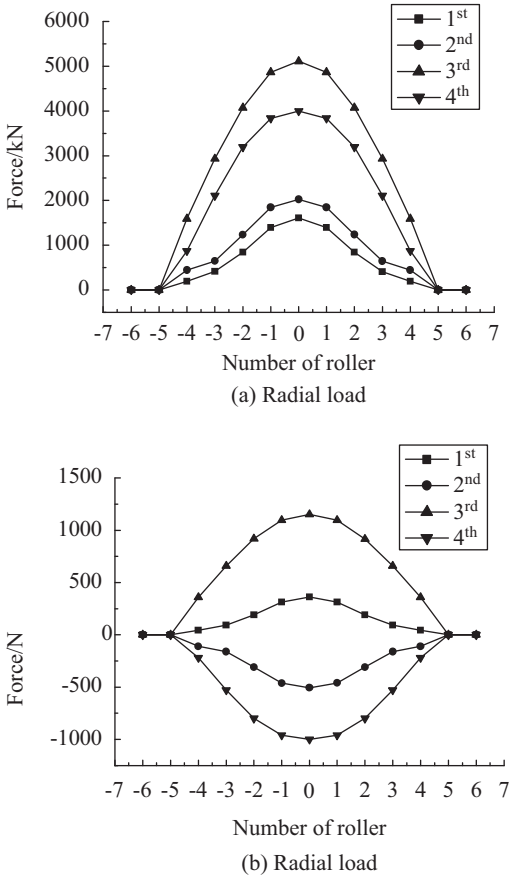


**Fig. 18. Load distribution of rollers using the T-BBEM.**

Table 3 indicates that the errors between the simulation result of the T-BBEM and the test result are less than 15%, and the errors between the simulation result of the GSC-BBEM and the test result are less than 10%, which is allowed in the simulation of engineering problems. Therefore, the validity and effectiveness of using the GSC-BBEM to solve the load distribution of bearings are proven.

## VI. CONCLUSIONS

This study presents a new method to analyze the load distribution of roller bearings using the Boundary Element Method. Based on geometrically similar conditions, all of the rollers

can be described as one object. Without considering the effects of friction, the load distribution of the roller bearings can be simulated with a three-object elastic contact BEM without friction. Bearing boundary elements are used to realize the discontinuous traction on the contact area, and the Hertz contact theory is used to revise the contact widths between the rollers and the bearing races.

The method is feasible for performing contact pressure distribution, load distribution and contact widths distribution between the rollers and the bearing races. The feasibility and validity of the method is certified by comparison with the traditional bearing-BEM and the experimental data.

## ACKNOWLEDGMENTS

This study is supported by the National Natural Science Foundation of China (Grant No. 51504157 and 51404159), Natural Science Foundation of Shanxi province (Grant No. 2015021110) and Youth Foundation of Taiyuan University of Science and Technology (Grant No. 20143009).

## REFERENCES

Bai, M. H. and H. B. Liu (1996). Basis of Engineering Elasticity. China Machine Press, Beijing. (in Chinese)

Chen, Z., J. H. Xiao and X. Yang (2010). Taylor series multipole boundary element-mathematical programming method for 3D multi-bodies elastic contact problems. International Journal for Numerical Methods in Engineering 83, 135-173.

Göncz, P., R. Potočnik and S. Glodež (2013). Computational model for determination of static load capacity of three-row roller slewing bearing with arbitrary clearances and predefined raceway deformations. International Journal of Mechanical Sciences 73, 82-92.

Gui, H. L., Q. Li, Q. X. Huang and G. X. Shen (2013). Analysis of contact problem using improved fast multipole BEM with variable elements length theory. Journal of Marine Science and Technology 21, 1-7.

Gun, H. and X. Gao (2014). Analysis of frictional contact problems for functionally graded materials using BEM. Engineering Analysis with Boundary Elements 38, 1-7.

Rodríguez-Tembleque, L. and R. Abascal (2010). A 3D FEM-BEM rolling contact formulation for unstructured meshes. International Journal of Solids and Structures 47, 330-353.

Segond, D. and A. Tafreshi (1998). Stress analysis of three-dimensional contact problems using the boundary element method. Engineering Analysis with Boundary Elements 22, 199-214.

Shen, G. X., X. D. Shu and M. Li (2001). The 3-D Boundary Element Method of Roller Bearing by Plate Element Analogue. Acta Mechanica Solida Sinica 14(3), 83-89.

Shu, X. D. and X. D. Xing (2004). Application of Sub-Element and Micro-Element in BEM for Load Distribution of mill bearing. Bearing 8, 5-8. (in Chinese, with English Abstract)

Waghole, V. and R. Tiwari (2014). Optimization of needle roller bearing design using novel hybird methods. Mechanism and Machine Theory 72, 71-85.

Wang, H. and S. Dai (2013). Study on contact Finite Element simulation of the high-angular contact thrust ball bearing. Computer Simulation 30(1), 305-309. (in Chinese, with English Abstract)

Wang, Y. S. and Q. Q. Yuan (2013). Contact force distribution and static load-carrying capacity of large size double row four-point contact ball bearing. Defence Technology 9, 229-236.

Xiao, H., X. Yang, Z. J. Chen and J. Wang (2010). Application of Hertz Contact Theory in Analyzing the Load Distribution of Mill Roller Bearing with Boundary Element Method. China Mechanical Engineering 21(21), 2532-2535, 2540. (in Chinese, with English Abstract)

Yang, X. and H. Xiao (2009). Three Dimension Multi-body Contact Boundary Element Method. Proceedings of the 2009 International Joint Conference on Computational Sciences and Optimization, Sanya, China, 652-655.

Yang, X., H. Xiao and Z. J. Chen (2014). Analyzing the Load Distribution of Mill Conical Roller with Bearing Boundary Element Method. Chinese Journal of Applied mechanics 31(1), 137-143. (in Chinese, with English Abstract)

Yu, C. X., G. X. Shen and D. Y. Liu (2005). Mathematical programming solution for the frictional contact mutipole BEM. Tsinghua Science & Technology 10(1), 51-56.

Zhang, Y. Q., Q. C. Tan, K. Zhang and J. G. Li (2012). Analysis of stress and strain of the rolling bearing by FEA method. Physics Procedia 24, 19-24.

Zhou, X. Y., H. R. Wang and Z. D. Jiang (2006). Influence of lubrication performance on the service life of rolling mill bearings. International Journal of Plant Engineering and Management 3, 184-192.